Photon count technique as a potential tool for insulation micro-defect detection: Principles and primary results

Xianhao Fan, Hanhua Luo, Fangwei Liang, Jun Hu, Weidong Liu, Chuanyang Li ✉ and Jinliang He ✉

ABSTRACT

The requirements for the construction of a new power system inevitably pose significant challenges and changes to the operation and maintenance of the power grid. To ensure the safe and stable operation of ultra-high voltage (UHV) transmission equipment, this work reports on the principles and preliminary results of using electroluminescence (EL)-based photon counting (PC) methods for early detection of micro-defects in GIS/GIL insulation spacer. In this study, the impact of voltage, gas pressure, and gas composition on the photon response of insulation is examined. Furthermore, the corresponding relationship between defect status and photon response characteristics is explored, along with the discussion of the EL mechanism and its evolution induced by defects. The research results demonstrate that PC measurement exhibits high sensitivity to variations in millimeter-scale defect size, position, and morphology at lower electric fields before partial discharge (PD) initiation. With this regard, this paper reveals promising prospects for the early detection of micro-defects in UHV transmission equipment using PC measurement-based methods.

KEYWORDS

Gas-insulated equipment, epoxy insulation, defect detection, partial discharge (PD), electroluminescence (EL).

With the aim of substantially elevating the transparency level of ultra-high voltage (UHV) transmission networks and augmenting the quality and efficacy of energy provisioning, the imperative of performing online state monitoring and diagnosis on critical UHV equipment has intensified. The broad application of epoxy-based insulating materials in gas-insulated equipment stems from their exceptional electrical and mechanical properties[1,2]. Nonetheless, the presence of diverse defects in the internal epoxy-based insulation components of GIL/GIS arises from a myriad of influencing factors, which result in the unexpected diagnosis of the equipment[3,4]. The precise detection of incipient insulation flaws has, therefore, emerged as a subject of extensive scholarly interest[5,6].

During insulation-charged operation, defects cause local electric field distortion[7]. When the electric field is strong enough to induce local breakdown near the defect, partial discharge (PD) will be triggered. At present, the prevailing method for defect detection and fault diagnosis involves analyzing diverse forms of PD signals[8–10]. However, micro-defects or the early stages of defect development may exhibit insufficient local field intensity to trigger PD. By the time obvious PD is observed, the insulation degradation has reached an irreversible phase. Findings demonstrated that, preceding PD initiation, charge carriers injected into the internal structure of insulating materials undergo migration under AC voltage excitation, and some of these carriers are captured by physical traps, thereby forming space charges[11,12]. Upon polarity reversal, newly injected charges combine with trapped carriers, leading to the emission of photons through radiative transitions, which manifests as electroluminescence (EL)[13]. An alternative explanation for EL activation under AC stress is offered by the double injection model[14]. The occurrence of EL in insulation provides evidence for the existence of latent harmful excited states. The surplus energy within systems can be dissipated through degradation pathways, thereby paving the way for chemical degradation processes[15]. Thus, the EL phenomenon activation preceding the initial occurrence of PD is considered a significant hallmark of the onset of insulation degradation[16]. In the previous work[17], the insulation pull rods used in GIS with surface scratches were utilized to verify the sensitivity and feasibility of the photon counting (PC) technique for mico-defect detection. The preliminary PC results show a positive correlation with the growing defect size, also, the potential theory to understand how defects promote the PC results is discussed. However, the recorded photons originated from both EL (occurs in insulation) and ionization/PD (occurs in surrounding air), it is, thus, hard to examine the EL property under the impact of various defects.

Given this issue, a comprehensive analysis of the micro-defect detection of epoxy-based insulation is carried out using PC. Firstly, specimens containing surface scratches, attached metal, and metal particle defects were fabricated. Subsequently, the photon response was systematically explored under various measurement conditions, encompassing pressure levels, gas categories, and applied voltages. Building upon this foundation, the mechanism of EL induced by defects and its nuanced influencing factors were examined based on the PC data acquired prior to the PD inception. Significantly, the findings highlight the profound impact of alterations in the defect state of specimens on the observed photon emission phenomena. Leveraging qualitative analysis, the correlations between the PC data and underlying defect characteristics can be established. Consequently, this investigation offers promising avenues for the detection and characterization of insulation defects in practical applications.

1 Experimental configuration and defect insulation specimen

Under AC voltage, the luminescence is constituted by the EL components (from insulation) and ionized components (released

Department of Electrical Engineering, Tsinghua University, Beijing 100084, China
Address correspondence to Chuanyang Li, chuanyang_li@tsinghua.edu.cn; Jinliang He, hejl@tsinghua.edu.cn

by recombination or PD of the ionized air near the insulation defect)[17]. However, the intensity of EL is at least two orders of magnitude smaller than that of the light generated by very small (<1 pC) PD[18]. Thus, discharges have to be avoided in the ambient and this is affected by increasing the pressure in the chamber to increase the discharge inception voltage[19].

To confirm the impact of pressure and category of ambient gas on the PC, the air, N_2, and SF_6 with 0.1 to 0.3 MPa are sequentially utilized. The photon counting is achieved via H8259-01 (Hamamatsu), and the working principle is shown in Figure 1(a). Also, the measurement platform is shown in Figure 1(b), 3 and 6 kV AC voltage with 50 Hz is used, respectively. An experimental cell is used to arrange the insulation specimens, a UHF sensor aims to confirm the inception voltage of PD, the signal acquisition card (PicoScope2000, with a sampling rate of 100 MS/s to 1 GS/s), and a personal computer is applied for recording the data. The measurement device and experimental setup are assigned in a light-tight condition inside an electromagnetic shielding room, with a dark count of less about 30 per second (pes) in SF_6.

In this work, alumina-doped epoxy resin is utilized to manufacture the shrinkage model for insulation spacer with the same physical dimension (height: 26 mm, diameter: 98 mm). The surface scratch (the length are 3, 5, and 7 mm, the width and depth are about 0.2 and 0.3 mm, the estimated volume are 0.18, 0.3, and 0.42 mm³), attached metal (same metal spikes, with a diameter of 1.0 mm and a length of 15 mm) with a different distance from metallic conductor (0, 15, and 30 mm), and metal particle (block particle with 0.5 and 1 mm diameter, 1.0 mm sphere particle) defect are artificially assigned in these specimens, as illustrated in Figure 1(c).

2 Measurement results and analysis

2.1 Impact of voltages on PC results

PC measurements were conducted on defect-free insulation spacers exposed to different environments (air, N_2, and SF_6) at 0.1 MPa.

The samples were subjected to step-up AC voltage (0, 3, 6 kV) for 800 seconds per stage. The presence of abundant residual space charges on the spacer surface led to turning direction and interfacial polarization under DC voltage, presenting as a decay followed by a stable curve in the photon counting spectrum[20]. However, the interfacial polarization process failed to complete within the cycle under 50 Hz AC voltage. To mitigate this, a prolonged withstand voltage (2000 s) was applied, incorporating charge injection and recombination mechanisms to deplete the residual space charges on the spacer surface, resulting in a stable emission curve with the average PC results for each excitation stage.

Analysis using an ultrahigh-frequency (UHF) sensor revealed the absence of PD initiation at 3 kV, as shown in Figure 2, but a notable enhancement in PC results was observed in Figure 3(a). During this stage, the average increase rate of the PC exceeded 300%, primarily attributable to the surface's EL and gas micro-ionization processes occurring at low field strengths. At 6 kV, distinct PD pulses were evident, corresponding to an average increase rate of the PC of 1562%. It is important to note that the PC does not correlate with the volume of the dielectric but with the electrical field[15]. Additionally, insulating gases exhibiting superior performance can effectively suppress ionization/PD processes, leading to a reduction in photon release levels. In the SF_6 environment, the PC values were less than 10% compared to those obtained in N_2.

2.2 Impact of gas pressure and gas category

EL is an important indicator of the health of insulating materials used in high-voltage applications, but photon release from air ionization and PD can interfere with its accurate measurement. A previous study demonstrated a sharp increase in photon counting results under PD, highlighting its potential impact on EL measurements[16]. To circumvent this issue, this study investigates the photon response characteristics of defect-free specimens under AC 3 kV and different pressures (0.1 to 0.3 MPa) in air, N_2, and SF_6 gases. The results revealed that increasing pressure significantly
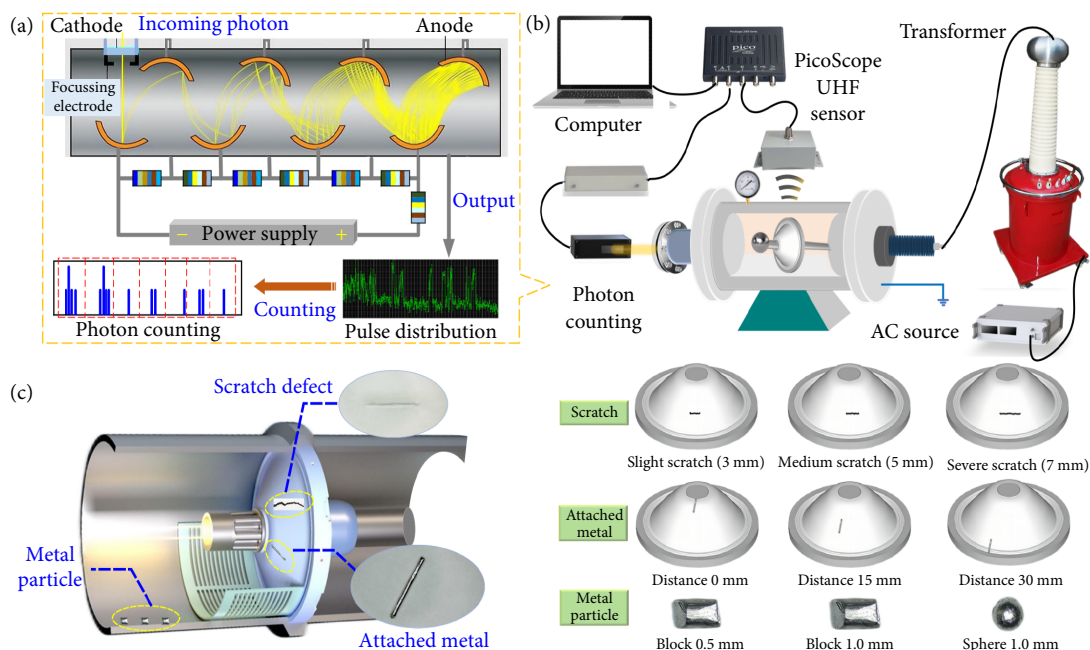

Fig. 1 The insulation specimen and measurement configuration. (a) Photon counting principle, **(b)** measurement configuration, and **(c)** prepared insulation spacer specimens with scratch, attached metal, and metal particle defects.
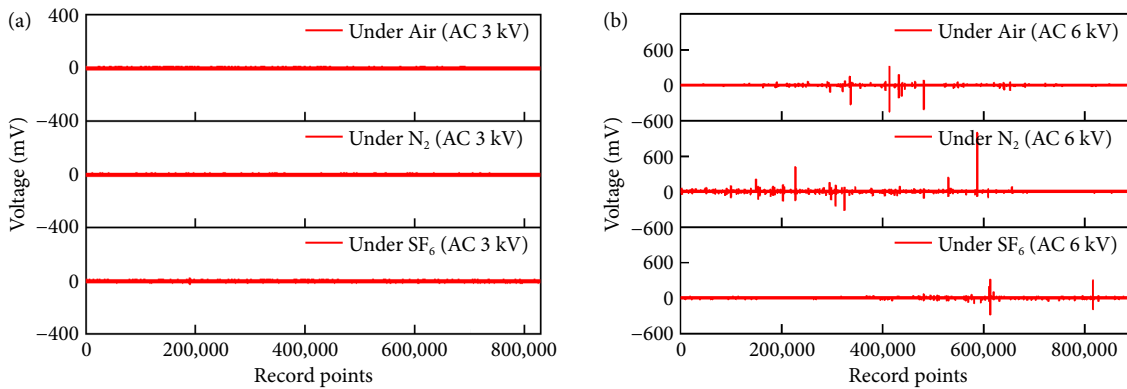
Fig. 2 **The recorded PD data during measurement. (a)** Defect-free specimen under AC 3 kV with 0.1 MPa gases, and **(b)** defect-free specimen under AC 6 kV with 0.1 MPa gases.
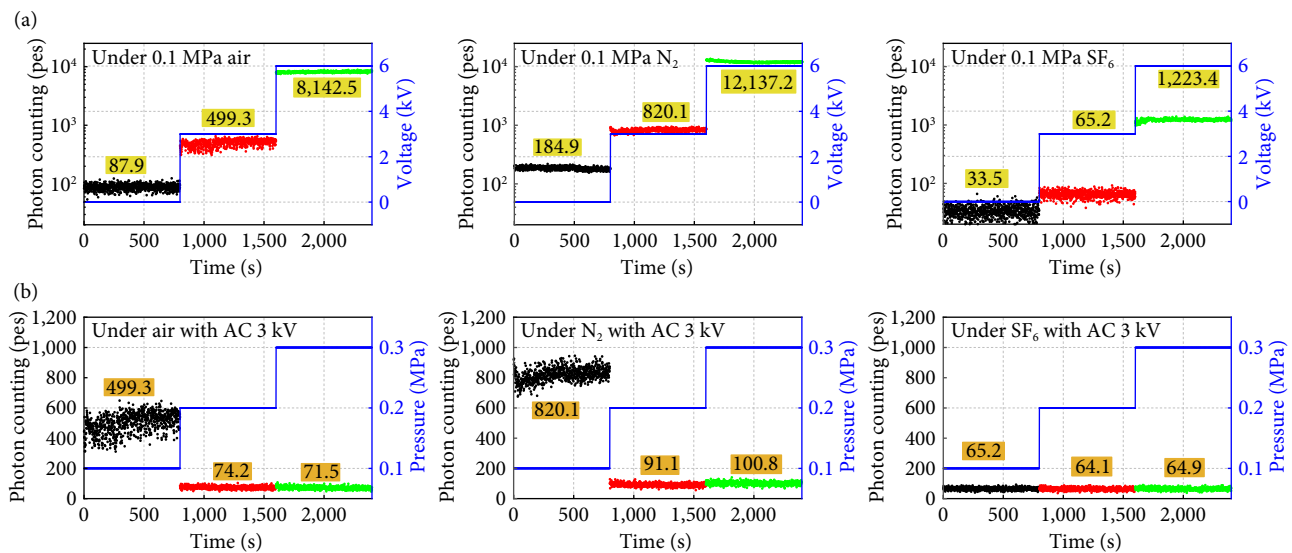

Fig. 3 **Photon counting results under different measurement conditions. (a)** Results versus voltage (0, 3, and 6 kV) corresponding to air, N_2, and SF_6, and **(b)** results versus atmospheric pressure (0.1 to 0.3 MPa) corresponding to air, N_2, and SF_6 under AC 3 kV.

raised the PD inception voltage for air and N_2, while suppressing photon release.

Notably, photons released by air ionization and PD contribute to more than 90% of luminescence, as evidenced by a substantial reduction in the number of photons detected in air and N_2 environments at higher pressure levels, which is in contrast to stable photon release levels observed in the SF_6 environment despite increased pressure. This phenomenon is attributed to the high stability of the S–F bond in SF_6 molecules, in which the bond energy of S–F is about 320 kJ/mol, while the N=N is about 230 kJ/mol and O=O is merely 145 kJ/mol. The high stability of SF_6 hinders their ionization and dissociation under higher electric field conditions than both N_2 and air, thus preserving insulation properties and suppressing PD inception[21]. Furthermore, the photons of specimens in different gas environments seem consistent after significantly increasing the gas pressure to 0.3 MPa, which means that similar photons are released by their EL process after eliminating PD's contribution to photon emission.

Figure 3(a) demonstrates distinct photon counts corresponding to an excitation voltage of 3 and 6 kV in N_2 and SF_6 environments, with the former exhibiting approximately 12.57 and 9.9 times higher photon emission than the latter. Remarkably, the discernible disparity in photon release persists even after accounting for PD contribution, as depicted in Fig 3(b). The N_2 environment

consistently manifests the highest photon count, while the SF_6 environment records the lowest. To delve further into this intriguing phenomenon, Figure 3(b) also presents the comparative analysis of photon counting results under AC 3 kV excitation for the same sample at identical gas pressures but differing gases. Notably, irrespective of PD exclusion, N_2 consistently outperforms both air and SF_6 in terms of photon emission levels.

This intriguing observation can be attributed, at least in part, to the distinct ionization energy requirements inherent to different gas molecules. The N_2 molecules possess a lower threshold for ionization, thereby enabling facile ionization upon receiving sufficient energy. Similar characteristics extend to N_2 and O_2 molecules in the air, wherein their ionization energies remain relatively low. Besides, the distribution ranges of PC results across distinct gas environments show the minimal breadth associated with SF_6. Notably, investigations demonstrate remarkable temporal stability of the EL intensity, a distinct departure from the observed discharge-controlled light emission[19]. Consequently, the prevailing mechanism responsible for light emission in the SF_6 stems from the process of EL on insulated surfaces.

2.3 Defect-dominated electroluminescence

The PC properties of ten specimens, comprising both defect-free and defective specimens, under AC 3 kV excitation in 0.1 MPa to

0.3 MPa are studied. The obtained measurement results are presented in Figure 4, accompanied by Table 1 statistical averages of PC across each defect stage, collectively revealing intriguing observations. Scratch defects, despite exhibiting varying lengths at constant locations, exhibit a clear positive correlation between surface scratch length and photon emission levels under different gas pressures when contrasted with the defect-free specimen. Notably, the 7 mm scratch defect sample records 2.5 times higher average PC than the defect-free specimen across distinct gas pressures.

In contrast, surface-attached metal defects that maintain a fixed size but alter their distance from the metal conductor exhibit unique photon emission properties based on their location. Specifically, the placement of surface metals at the metal-insulation-gas triple interface leads to higher photon counts than those located in the middle of the dish. Additional findings indicate an increased photon count in metal particle defects of identical shape linked to an increase in particle size. Remarkably, among particles of identical size, spherical particles display lower photon counts than chunky metal particles due to a lower degree of electric field distortion resulting from their larger curvature radius.

3 Discussion

Upon external electric field surpassing the threshold level, Schottky law-based electron and hole injection from the electrode into the dielectric material generate free charge carriers that undergo diffusion and migration behaviors[22]. Charge carrier types can be classified as either mobile or trapped electron or hole, with mobile carriers being linked to conduction through physical traps resulting from the disordered structure, as well as deep traps, described by chemical traps, allowing charges to escape via thermal activation[23]. Physical response processes during charge carrier migration correlate with carrier energy levels, in which charge recombination does not require any threshold and can occur at a low electrical field[19]. Mobile space charges possessing kinetic energy of 1.5 gap energy (E_g) can generate electron-hole pairs via impact ionization, while electronically excited states can be induced by electrons with kinetic energy below the ionization energy level[24]. As to the applied 50 Hz AC voltage, charge injection into the dielectric proceeds mainly concentrated in the surface layer of insulation material. This makes either collision excitation/ionization or migration-driven recombination challenging, the injection and recombination of charge carriers trigger EL on the condition that electrode-insulation interfaces alternately act as an anode and cathode. With
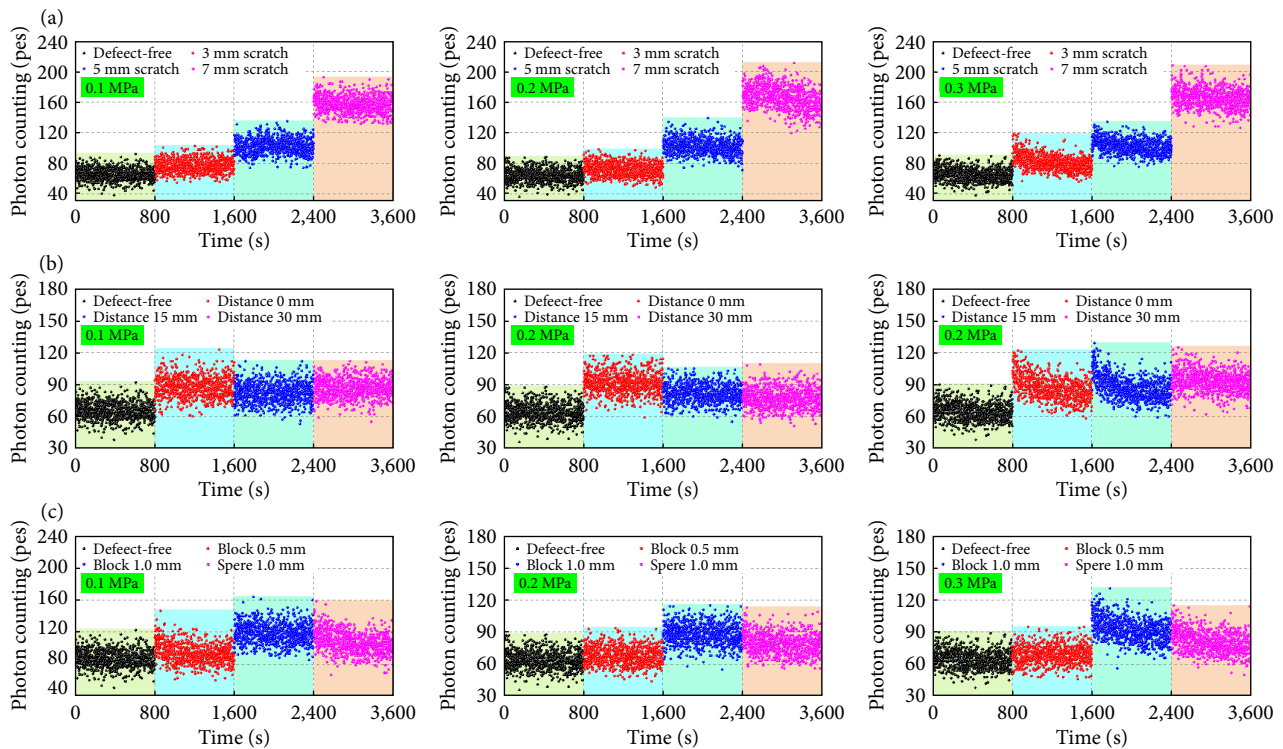

Fig. 4 Defect-dominated photon counting results. (a) Results of surface scratch (with the length in 3, 5, and 7 mm) under 0.1 to 0.3 MPa, **(b)** results of attached metal (distance from metal conductor 0, 15, and 30 mm) under 0.1 to 0.3 MPa, **(c)** results of metal particles (block particles with 0.5 and 1 mm diameter, sphere particles with 1 mm diameter) under 0.1 to 0.3 MPa.

Table 1 Propellant masses vs. transfer time using orbital averaging and guidance scheme

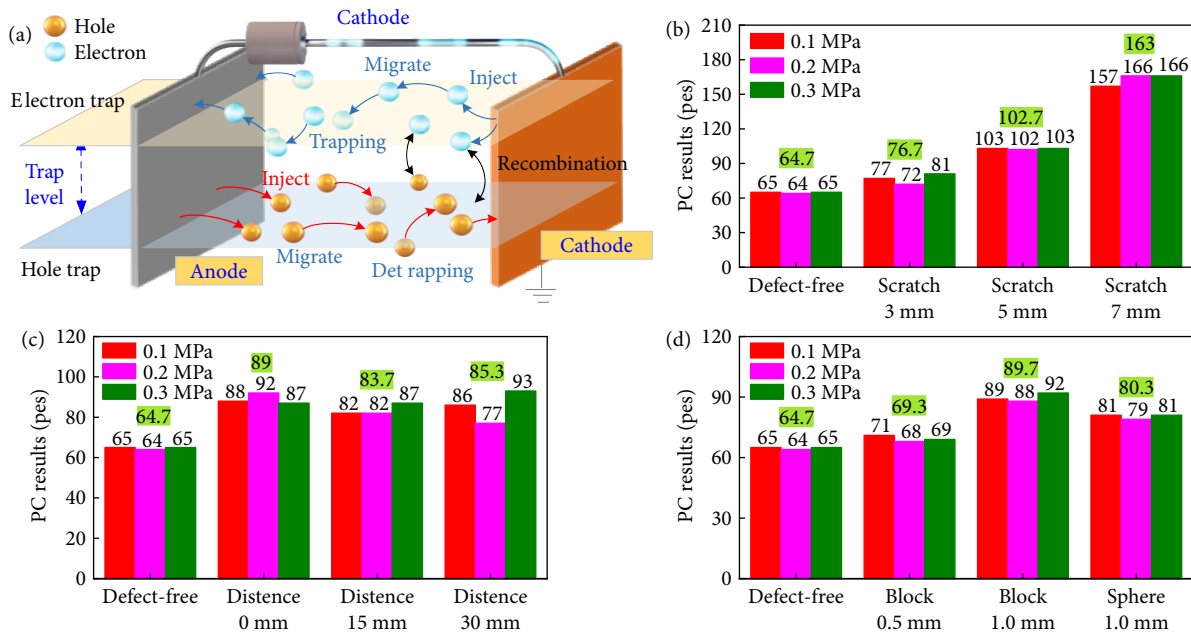| Pressure (MPa)	Defect free	Surface scratch			Attached metal			Metal particles		
		3 mm	5 mm	7 mm	0 mm	15 mm	30 mm	Block 0.5 mm	Block 1.0 mm	Sphere 1.0 mm
0.1	65	77	103	157	88	82	86	71	89	81
0.2	64	72	102	166	92	82	77	68	88	79
0.3	65	81	103	166	87	87	93	69	92	81
Average value	65	77	102	163	89	84	86	69	90	80

Fig. 5 **(a)** Response behavior of charge carriers induced by defects, **(b)** the distribution of PC of scratch defect, **(c)** the distribution of PC of attached metal defect, and **(d)** the distribution of PC of metal particle defect.

Figure 3(a) supported observation, the EL mechanism under voltage increase from 0 to 6 kV can be categorized into: (i) the initial injection/recombination process close to the interfaces, followed by (ii) injected carriers leading to either interfacial or bulk-based recombination, and (iii) impact/ionization or hot electrons could take place, as illustrated in Figure 5(a).

The mechanism of defect-induced EL follows the aforementioned three-stage evolution process. However, the presence of defects can alter the surrounding electric field distribution and charge accumulation concentration, thereby affecting the photon emission. The relevant simulation model would help understand the impact rule caused by various defects on the distribution of electric field and charge concentration[7, 25, 26]. Rely on the average PC under different air pressures shown in Table 1, trend charts of photon variation corresponding to three types of defects were plotted in Figures 5(b) to 5(d). For scratch defects, the appearance of scratches leads to local electric field distortion and changes in the energy level distribution of the insulating surface, resulting in more space charges and charge accumulation. Therefore, the recombination process is promoted, demonstrating a positive correlation with scratch length. By establishing the functional relationship between photon counts and scratch length, quantitative analysis of severe states of such defects is expected to be achieved.

Similarly, the influence of defect position and shape on the partial discharge (PD) results can also be attributed to their impact on the surrounding electric field strength. However, this behavior is mainly achieved by intensifying the degree of air ionization near the defects and does not significantly affect the intensity of electroluminescence inside the insulation. To verify the contained mechanism behind EL, one effective approach involves investigating wavelength-intensity spectra and subsequently calculating the associated energy levels during radiative transitions[27]. The findings demonstrated that light emission originating from discharges manifests a pronounced peak in the ultraviolet region of the optical spectrum[16]. The EL spectrum arising from the recombination of electrons and holes trapped at deep trapping centers within the bulk of the insulation is found to extend from the visible region towards the UV region, exhibiting notably higher energy

levels compared to those occurring at the insulation-electrode interface[28]. The energy range corresponding to collision-induced ionization/excitation lies between that of local discharge events and recombination processes.

4 Conclusions

This work investigates the PC characteristics of insulation spacers with surface scratches, attached defects, and metal particle defects. The influence of excitation voltage, gas pressure, and gas composition is discussed sequentially. Findings indicate that photon release at lower field strengths is primarily attributed to EL and gas micro-ionization, with over 90% of photon emissions originating from PD inception. Increasing gas pressure effectively suppresses the inception electric field of PD for different gases, thereby mitigating the influence of PD-induced photons on EL measurements.

The evolution process of the dominant EL mechanism follows a three-stage progression dominated by electric field intensity. EL contributions in the experimental environment derive from the electrode-insulation interface, defect regions, and gas ionization near defects. The size, position, and shape of defects impact the level of photon release, attributable to distortion in the surrounding electric field or changes in charge density. Present results demonstrate a preliminary functional relationship between average photon counts and defect severity, suggesting the potential for quantitative defect analysis. With this regard, future research should focus on defect-type identification methods based on photon counting measurements.

Article history

Additional information

Declaration of competing interest

The authors have no competing interests to declare that are relevant to the content of this article.

References

[1] Li, C., Zhang, C., Lv, J., Liang, F., Liang, Z., Fan, X., Riechert, U., Li, Z., Liu, P., Xue, J., et al. (2022). China's 10-year progress in DC gas-insulated equipment: From basic research to industry perspective. *iEnergy*, 1: 400–433.

[2] Li, C., Yang, Y., Xu, G., Zhou, Y., Jia, M., Zhong, S., Gao, Y., Park, C., Liu, Q., Wang, Y., et al. (2022). Insulating materials for realising carbon neutrality: Opportunities, remaining issues and challenges. *High Voltage*, 7: 610–632.

[3] Wang, F., Liang, F., Zhong, L., Chen, S., Li, C., Xie, Y. (2021). Short-time X-ray irradiation as a non-contact charge dissipation solution for insulators in HVDC GIS/GIL. *IEEE Transactions on Dielectrics and Electrical Insulation*, 28: 704–709.

[4] Yadam, Y. R., Sarathi, R., Arunachalam, K. (2022). Numerical and experimental investigations on influence of internal defect parameters on partial discharge induced UHF signals in gas insulated switchgear. *IEEE Access*, 10: 110785–110795.

[5] Wang, F., Wang, L., Chen, S., Sun, Q., Zhong, L. (2021). Effect of profiled surface on streamer propagation and the corner effect. *IEEE Transactions on Dielectrics and Electrical Insulation*, 28: 2186–2194.

[6] Fan, X., Liang, F., Luo, H., Li, C., Liu, J., He, J. (2023). Adaptive-optimization-based digital simulation database for nonuniform aging diagnosis of transformer insulation system. *IEEE Transactions on Industrial Electronics*, https://doi.org/10.1109/TIE.2023.3296764.

[7] Talaat, M., El-Zein, A., Amin, M. (2018). Electric field simulation for uniform and FGM cone type spacer with adhering spherical conducting particle in GIS. *IEEE Transactions on Dielectrics and Electrical Insulation*, 25: 339–351.

[8] Han, X., Zhang, X., Guo, R., Wang, H., Li, J., Li, Y., Zhao, M. (2022). Partial discharge detection in gas-insulated switchgears using sensors integrated with UHF and optical sensing methods. *IEEE Transactions on Dielectrics and Electrical Insulation*, 29: 2026–2032.

[9] Chen, W., Wang, J., Wan, F., Wang, P. (2019). Review of optical fibre sensors for electrical equipment characteristic state parameters detection. *High Voltage*, 4: 271–281.

[10] Hashim, A. H. M., Azis, N., Jasni, J., Radzi, M. A. M., Kozako, M., Jamil, M. K. M., Yaakub, Z. (2023). Application of ANFIS and ANN for partial discharge localization in oil through acoustic emission. *IEEE Transactions on Dielectrics and Electrical Insulation*, 30: 1247–1254.

[11] Zhu, X., Zhou, G., Yin, Y. (2023). Numerical simulation of trap modulated multi-mobility charge transport under AC field. *IEEE Transactions on Dielectrics and Electrical Insulation*, 30: 681–689.

[12] Shimakawa, H., Kumada, A., Hidaka, K., Sato, M., Yasuoka, T., Hoshina, Y., Shiiki, M. (2021). One-dimensional modeling of charge transport in epoxy for DC-GIS insulating spacer. *IEEE Transactions on Dielectrics and Electrical Insulation*, 28: 1457–1464.

[13] Qiao, B., Teyssedre, G., Laurent, C. (2016). Electroluminescence and cathodoluminescence from polyethylene and polypropylene films: Spectra reconstruction from elementary components and underlying mechanisms. *Journal of Applied Physics*, 119: 024103.

[14] Bamji, S. S., Bulinski, A. T., Densley, R. J. (1988). Threshold voltage of luminescence and electrical tree inception in low-density polyethylene. *Journal of Applied Physics*, 63: 5841–5845.

[15] Mary, D., Albertini, M., Laurent, C. (1997). Understanding optical emissions from electrically stressed insulating polymers: Electroluminescence in poly(ethylene terephthalate) and poly(ethylene 2, 6-naphthalate) films. *Journal of Physics D: Applied Physics*, 30: 171–184.

[16] Li, C., Hu, J., Lin, C., Zhang, B., Zhang, G., He, J. (2016). Fluorine gas treatment improves surface degradation inhibiting property of alumina-filled epoxy composite. *AIP Advances*, 6: 025017.

[17] Fan, X., Niu, S., Luo, H., Liang, J., Liu, F., Li, W., Liu, W., Gao, W., Huang, Y., Li, C., et al. (2023). Photon counting technique as a potential tool in micro-defect detection of epoxy insulation pull rod in GIS. *High Voltage*, https://doi.org/10.1049/hve2.12388.

[18] Bamji, S., Bulinski, A., Abou-Dakka, M. (2009). Luminescence and space charge in polymeric dielectrics -[whitehead memorial lecture (2008). *IEEE Transactions on Dielectrics and Electrical Insulation*, 16: 1376–1392.

[19] Laurent, C., Massines, F., Mayoux, C. (1997). Optical emission due to space charge effects in electrically stressed polymers. *IEEE Transactions on Dielectrics and Electrical Insulation*, 4: 585–603.

[20] Mary, D., Malec, D. (2006). Change in electroluminescence activity in polymers prior to AC dielectric breakdown. In: Proceedings of the 2006 IEEE Conference on Electrical Insulation and Dielectric Phenomena, Kansas, MO, USA.

[21] Long, Y., Guo, L., Shen, Z., Chen, C., Chen, Y., Li, F., Zhou, W. (2019). Ionization and attachment coefficients in C_4F_7N/N_2 gas mixtures for use as a replacement to SF_6. *IEEE Transactions on Dielectrics and Electrical Insulation*, 26: 1358–1362.

[22] Le Roy, S., Teyssedre, G., Laurent, C. (2005). Charge transport and dissipative processes in insulating polymers: Experiments and model. *IEEE Transactions on Dielectrics and Electrical Insulation*, 12: 644–654.

[23] Le Roy, S., Segur, P., Teyssedre, G., Laurent, C. (2004). Description of bipolar charge transport in polyethylene using a fluid model with a constant mobility: Model prediction. *Journal of Physics D: Applied Physics*, 37: 298–305.

[24] Laurent, C. (1999). Optical prebreakdown warnings in insulating polymers. *IEEE Electrical Insulation Magazine*, 15: 5–13.

[25] Deng, Y., Fan, X., Luo, H., Wang, Y., Wu, K., Liang, F., Li, C. (2023). Impact of air gap defects on the electrical and mechanical properties of a 320 kV direct current gas insulated transmission line spacer. *Energies*, 16: 4006.

[26] Li, X., Cao, C., Lin, X. (2022). Influence of conducting particle on DC flashover characteristics and tracking property of GIS/GIL insulator. *IEEE Access*, 10: 17212–17220.

[27] Qiao, B., Teyssedre, G., Laurent, C. (2015). Uncover the electroluminescence in wide band gap polymers. *Journal of Physics D: Applied Physics*, 48: 405102.

[28] Mizuno, T., Liu, Y. S., Shionoya, W., Yasuoka, K., Ishii, S., Miyata, H., Yokoyama, A. (1997). Electroluminescence in insulating polymers in ac electric fields. *IEEE Transactions on Dielectrics and Electrical Insulation*, 4: 433–438.